Atomistic study on effects of solute atoms on energy profile of edge dislocation mobility in FCC-Cu alloys

Authors

Chiharu Kura [a, *], Masato Wakeda [b, *], Kazushi Hayashi [a], Takahito Ohmura [b]

Affiliations

[a]Applied Physics Research Laboratory, Kobe Steel, Ltd., 1-5-5 Takatsukadai, Nishi-ku, Kobe 651-2271, Japan

[b]Research Center for Structural Materials, National Institute for Materials Science, 1-2-1 Sengen, Tsukuba, Ibaraki 305-0047, Japan

* Corresponding authors.

E-mail addresses: kura.chiharu@kobelco.com (C. Kura)

and WAKEDA.masato@nims.go.jp (M. Wakeda).

Abstract

Solid-solution strengthening is an effective method to increase the mechanical strength of metal alloys. Revealing the solid-solution strengthening mechanism based on the energy profile of the dislocation motion is vital for the non-empirical development of high-strength metal alloys. This study provides detailed energy profiles (i.e., energy surfaces) of the edge dislocation gliding motion under the effect of solute atoms, as well as the atomic-scale origin of solute strengthening in face-centered cubic (FCC) Cu alloys. The maximum shear stress (τ_{max}) required for the dislocation to leave the solute atoms (Ni, Co, and Mo, all with different sizes and stacking fault effects) was qualitatively evaluated by finite temperature molecular dynamics simulations. By the nudged elastic band (NEB) analysis, we determined the atomistic origin of the energy barrier for the edge dislocation motion and the maximum force required to overcome the solute pinning effect (i.e., depinning force, F_{NEB}) in binary Cu alloys. By linking F_{NEB} to the size misfit, a theoretical prediction model based on size effects and the volumetric strain field was used and can qualitatively explain the increment in the maximum shear stress ($\Delta\tau_{max}$) by the solute atoms. These results provide an atomistic basis for the prediction of the solute-strengthening effect correlated with the edge dislocation motion in wide FCC systems.

1. Introduction

Face-centered cubic (FCC)-Cu alloys have been used in industrial products because of their mechanical strength and electrical conductivity [1-4], and various Cu alloys with improved their properties have been developed [5-9]. Solid-solution strengthening, which is one of the strengthening mechanisms [10-13], is induced by the interaction between dislocations and solute atoms [14,15]. Its role in FCC metals has been discussed based on yield stress measurements from experimental tensile tests [16,17], first-principles calculations [18-20], and molecular dynamics (MD) simulations [21-23]. The atomistic origin of solid-solution strengthening is likely from the energy barriers for the dislocation glide motion created by solute atoms. These energy barriers can be evaluated by the nudged elastic band (NEB) method, which searches for the minimum energy path (MEP) between two states in the coordination space [24-26]. In general, FCC metals have a lower Peierls barrier and stress than body-centered cubic (BCC) metals, and dislocations in FCC metals decompose and expand into two partial dislocations with a stacking fault (SF) [27]. Through the expanded dislocation core structure in FCC metals, the solute atoms can interact with SF (Suzuki effect) and partial dislocations [28, 29], thereby affecting the energy profile (or energy surface) of the dislocation motion.

The dislocation-solute atom interaction in FCC metals is believed to depend on multiple factors, including the size and SF effects. Therefore, it is important to acquire atomistic knowledge of the solute effect on the energy profile of the edge dislocation glide motion while also considering the individual effects of the solute-partial dislocation interaction and solute-SF interaction for controlling plastic deformation in FCC metals. In this study, we focused on the effects of solute elements on the edge dislocation motion and investigated the origin of the interaction between edge dislocations and solute atoms in FCC-Cu alloys induced by a volumetric strain (size effect) and SF (SF effect) through atomistic simulations. In addition to MD simulations of the dislocation dynamics analyses, we evaluated the energy profiles of the edge dislocation motion via the NEB method to investigate the dislocation-solute atom interaction, and used a theoretical model that can predict the depinning force obtained from the energy profiles.

2. Materials and methods

In this study, FCC-Cu models containing an edge dislocation were constructed and replaced one or more Cu atoms with solute atoms. We investigated the dislocation-solute atom interaction by MD simulations at a finite temperature and through the NEB method at 0 K. Furthermore, we discussed the atomic size and Suzuki effects of the solute

atom on the solid-solution strengthening and on the energy profile for dislocation motion. The pure Cu model had dimensions of 25.6, 1.32, and 12.5 nm in the *x*, *y*, and *z* directions, respectively. The crystallographic orientations were *x* $[1\bar{1}0]$, *y* $[11\bar{2}]$, and *z* $[111]$. The model dimension along the *y* direction was equivalent to 3*l*, where *l* (= 4.43 Å) is the unit length along *y* direction. The model contained 33,000 atoms. LAMMPS and OVITO were used for the MD simulations and visualization of the atomic structure [30, 31]. In order to clearly show the interaction between an edge dislocation and a solute atom, we visualized the dislocation motion from $[11\bar{2}]$ direction.

The edge dislocation with the $[11\bar{2}]$ line vector is on the (111) slip plane with a Burgers vector $\boldsymbol{b} = a/2[1\bar{1}0]$, where a is the lattice constant. Fig. 1(a) shows the dislocation core structure after structural relaxation, where a perfect edge dislocation dissociates into two partial dislocations connected by a SF. Relaxation was performed using MEAM potentials [32,33], which are one of the most widely used potentials in metals and metal alloy systems. We actually observed a perfect dislocation with a dissociated core structure after relaxation (Fig. 1(b)). Therefore, these simulation models reasonably reproduced the edge dislocation core structure of FCC-Cu.

Fig. 2(a) shows the distribution of the atomic volume around the edge dislocation in the pure Cu model. The atomic volumetric strain (ε_v) was compressive in the *z*-axis

positive direction and tensile in the *z*-axis negative direction from the center of the model. Fig. 2(b) summarizes the atomic volumetric strain variations along the *x*-axis in the vicinity of the edge dislocation core represented in Lines 1-4 in the lower panel of Fig. 2(a). A large compressive ε_v was observed in Lines 1 and 2, whereas a large tensile ε_v was observed in Lines 3 and 4, compared with the ε_v far from the dislocation. ε_v with a large magnitude appeared around the partial dislocations. We defined the maximum value of ε_v for each line in Lines 1-4 as ε_V^{max} and have indicated them in Fig. 2(b) for later discussion.

Figure 3(a) shows the solute effects on the changes in Ω and the solute effect on the stacking fault energy (SFE) ($\Delta\gamma_{SF}$); inset atomic images are a model with 108 atoms to evaluate the size effect (Ω) and a model with 180 atoms to evaluate the SF effect. MEAM potentials [32,33], which describe Cu-Ni, Cu-Co, and Cu-Mo systems with different size and chemical effects on the SFE and the interaction energies (or segregation energies), were used for the binary model systems. Two FCC models, Cu_{108} and $Cu_{107}X_1$, where *X* is the solute atom (i.e., *X* = Ni, Co, Mo) were used to evaluate the size effects of Ω. The atomic configuration and cell volume of the models were relaxed at 0 K using the conjugate gradient method, and the size effects were obtained using Equation (1):

$$\Omega = n\{V(\mathrm{Cu}_{107}X_1) - V(\mathrm{Cu}_{108})\}/V(\mathrm{Cu}_{108}) \quad (1)$$

where $V(Cu_{108})$ and $V(Cu_{107}X_1)$ represent the volumes of the Cu_{108} and $Cu_{107}X_1$ models after structural relaxation, respectively, and n is the number of atoms in the model (i.e., n = 108). The stacking fault energy (γ_{SF}) was calculated using Equation (2):

$$\gamma_{SF} = (E_{SF} - E_{FCC})/S \quad (2)$$

where E_{FCC} and E_{SF} are the energies of the model without and with SF, respectively, and S is the area of the SF. $\Delta\gamma_{SF}$ was calculated from the γ_{SF} of the Cu_{180} and $Cu_{179}X_1$ models (solute atom X was on the SF plane) using Equation (3):

$$\Delta\gamma_{SF} = \gamma_{SF}(Cu_{179}X_1) - \gamma_{SF}(Cu_{180}) \quad (3)$$

Additional information of the models for Ω and $\Delta\gamma_{sf}$ calculations can be found in Fig. S1 and Fig. S2 in the Supplementary Material.

The size and SF effects on the energy profile of the dislocation motion differed according to the model system (Fig. 3(a)). Cu-Ni exhibited small size and SF effects. In addition, Cu-Ni with the EAM potential [34] was also evaluated, and a similar tendency to that of the MEAM potential was observed. This result indicates that the size and SF effects in Cu-Ni were small. The size and SF effects of Co were similar to those of Ni. In contrast, Mo had larger size and SF effects than Co and Ni. Note that here, we used these model systems to qualitatively evaluate the size and SF effects on the energy profile of the edge dislocation motion rather than to obtain precise material properties of real Cu

alloys. Using this model systems, we also intend to propose a theoretical basis for the effect of solute atoms on the energy profile for the edge dislocation motion and the origin of solid-solution strengthening based on discretized solute effects (i.e., size and SF effects). Fig. 3(b) shows the distribution of the interaction energy (E_{int}) around the dislocation core. E_{int} was defined as zero when the solute atom was located far from the dislocation core and had a negative value when the dislocation-solute atom interaction was attractive. Based on these definitions, E_{int} can also predict segregation behaviors, where a negative E_{int} indicates that the solute atoms prefer to segregate at the site. As shown in Fig. 3(b), Mo tends to segregate in the tensile volumetric strain region around the partial dislocations. In contrast, Ni and Co have a lower E_{int} than Mo. The atomic radii of Mo, Co, and Ni obtained by first-principles calculations were in the order of Mo > Co ≈ Ni ≈ Cu [35], and agreed well with those obtained in the simulations of the present study, revealing a small size misfit in Cu-Ni and Cu-Co and a large misfit in Cu-Mo.

3. Results and Discussion

3.1 Solute-strengthening effect evaluated using MD simulations

To investigate the solute-strengthening effect of the models in this study, we conducted MD simulations at finite temperatures and applied a shear stress along the *x*-

axis on the *z*-plane of the atomic models to move the edge dislocation. Fig. 4(a) shows an example of the dislocation motion under the effect of a solute atom in Cu-Mo when Mo is in Line 3 (the interaction processes are shown in Fig. S3 in the Supplementary Material). The maximum stress (τ_{max}) required for the dislocation to move away from the solute atom (i.e., depinning) was determined by increasing the applied shear stress. The temperature for the MD simulations was 10 K, and a Cu atom in Lines 1-4 was replaced with the solute atom. The atomic model was initially relaxed for 100,000 steps without a shear stress, following which the shear stress was increased by 1 MPa every 2,000 steps.

Fig. 4(b) shows $\Delta\tau_{max}$ for Lines 1-4, where $\Delta\tau_{max}$ is the difference in τ_{max} between the solute system and pure Cu. The $\Delta\tau_{max}$ values of Cu-Ni and Cu-Co are almost zero, regardless of the line position. These results can be explained by the small size and SF effects of Ni and Co, as previously shown in Fig. 3. We created another model containing five Co atoms in Line 3, and the maximum pinning effect appeared. This result suggests that the pinning effect is also induced if multiple solute atoms simultaneously interact with the partial dislocation or SF region. There is a possibility that magnetic properties of Ni and Co atoms affect dislocation-solute atom interactions. However, the effect of magnetic properties should be treated by the first-principles calculations with large scale

computation and beyond the scope of the current study, in which only the size and SF effects are focused.

The results obtained for Cu-Mo differed from those for Cu-Co and Cu-Ni. The $\Delta\tau_{max}$ significantly varied depending on the Mo position, with the highest value obtained when Mo was in Line 3. For Cu-Mo, the thickness dependence of the *y*-axis and temperature dependence of $\Delta\tau_{max}$ were further investigated. Additional MD simulations were performed for models with *y*-axis lengths of 1*l* and 5*l* to investigate the dependence of the *y*-axis length (i.e., the model dimension along the dislocation line direction). $\Delta\tau_{max}$ increased with decreasing *y*-axis length because of the increase in the solute concentration. Shear MD simulations for Cu-Mo with Mo in Line 3 were also performed at 50, 100, 300, and 500 K, as shown in the inset. τ_{max} decreased with increasing temperature, suggesting that depinning is essentially a thermally activated process, which can be generally expressed by the transition state equation $\nu\exp(-G/k_BT)$; T, ν, k_B, and G denote the temperature, trial frequency, Boltzmann constant, and activation energy, respectively. In later sections, we directly obtained G and the depinning force from the energy profile using the NEB method at 0 K and discussed the individual size and SF effects on G. It is possible that the temperature alters the size effect, SF effect, and activation energy in a high-temperature range. The temperature dependence of the activation energy is an

important and interesting topic for high-temperature material strength studies. However, in the current study, as a first step, we focused only on the dislocation behaviors dominated by the energy barrier at 0 K obtained by the NEB method.

3.2 Energy profile diagram evaluated by the NEB method

The energy profiles of the edge dislocation motion under the effect of a solute atom were obtained using the NEB method, which provided a more detailed assessment of the size and SF effects. Figs 5 and 6 show the potential energy profile and visualization of the relative position between a dislocation and solute atom for Cu-Co and Cu-Mo. There is no significant difference in the potential energy of Cu-Co with one Co atom (Fig. 5(a) and (b)), even when the Co atom is close to the partial dislocations ((ii) and (iv)) or in the interior of the SF (iii). The observed energy changes are less than 10^{-1} eV, suggesting that Co had a small effect on the edge dislocation motion. The results for Cu-Ni were similar to those for Cu-Co (Fig. S4 in the Supplementary Material). To discuss the effect of multiple Co atoms, NEB calculations for the Cu model containing five Co atoms in Line 3 were also conducted (Fig. 5(c) and (d)). A negative potential energy profile (–0.1 eV) was observed when the Co atoms were in the SF region (i.e., dislocation position (iii)). However, no potential energy change was observed when the partial

dislocations were close to the Co atoms. Because the SF is a planar fault, it may contain several solute atoms which promote the dislocation-solute atom interaction. Therefore, even if the interaction between a SF and single solute atom is small, the existence of multiple solutes in the SF region can induce the pinning force for the edge dislocation and contribute to solute strengthening, as shown in Fig. 4(b).

Fig. 6 shows the NEB results for Cu-Mo. Two typical energy profiles are obtained depending on the Mo position. When Mo is located in Line 1 or 2, close to the partial dislocations, the energy changes are positive (+0.2 and +0.38 eV, respectively). Energy changes of +0.01 and +0.08 eV are also observed in the SF region. In contrast, the potential energies are negative when Mo is in Line 3 and Line 4, particularly when Mo interacts with the partial dislocations (-0.6 eV and -0.28 eV, respectively). A negative potential energy is also observed when Mo is in the SF, but with a value approximately 1/10 that of the interaction energy between the partial dislocation and Mo. These significant changes in the energy profile and the interaction between the partial dislocation and solute Mo are reasonable when considering that Mo has a larger atomic volume than Cu [35]. Although Mo also has a considerable effect on the SFE in the current model system, the interaction with the SF is smaller than that with partial dislocations.

3.3 Depinning force evaluated by the energy profile and a prediction model for the depinning force

The origin of solid-solution strengthening in FCC metals and a prediction model for the depinning force obtained by the NEB method are discussed in this section. We focused on the solute Mo, which has large size and SF effects in the current model system. The depinning force at which the edge dislocation leaves from the solute atom can be estimated from the slope of the energy profile obtained from the NEB method. Fig. 7 shows the depinning force estimated from the NEB results, F_{NEB}. Fig. 7(a) shows that depinning is dominated by the slope between points A and B, which exhibits the maximum energy difference (E(B) – E(A)) between two neighboring points in the NEB energy profile. The positions of two partial dislocations, denoted by x_1(A) and x_2(A) for point A and x_1(B) and x_2(B) for point B, were obtained by visualizing the dislocation core structure (Fig. 7(b)). The position of the dislocation of points A and B, denoted by x(A) and x(B), respectively, was defined as the center of the two partial dislocations as x(A)={x_1(A)+x_2(A)}/2 and x(B)={x_1(B)+x_2(B)}/2. Consequently, the F_{NEB} necessary to overcome the energy slope between points A and B can be calculated using the following equation (4):

$$F_{NEB} = \{E(B)-E(A)\}/\{x(B) -x(A)\} \quad (4)$$

Fig. 7(c) shows F_{NEB} as a function of $|\varepsilon_{\mathrm{V}}^{\max}|$ in Lines 1-4, which is defined in Fig. 2(b). The linear alignment of the F_{NEB} plots shows a clear correlation between $|\varepsilon_{\mathrm{V}}^{\max}|$ and F_{NEB}, suggesting that the depinning force is mainly dominated by the size effect even if Mo has a large SF effect. In reality, the maximum slope in the energy profile is caused by the interaction between the partial dislocation and a solute atom. Because the edge dislocation has a large volumetric strain around the partial dislocations, the dislocation-solute atom interaction in FCC metals is mainly caused by the size effect if the solute atom has a large size misfit. Based on this, a theoretical model for predicting the depinning force necessary to overcome the size effect (F_{V}) is expressed by the following equation (5):

$$F_{\mathrm{V}} = \alpha|\Omega|Gb^2|\varepsilon_{\mathrm{V}}^{\max}| \quad (5)$$

where Ω, G, and b represent the size effect, shear stress, and norm of the Burgers vector, respectively. α is a fitting parameter, and is obtained as 0.89. The relationship between F_{V} and $\varepsilon_{\mathrm{V}}^{\max}$ is denoted by the dashed line in Fig. 7(b), in which F_{NEB} and F_{V} are quite similar. This result also supports the hypothesis that the dislocation-Mo interaction originates from the size misfit [35]. We also evaluated ε_{v} in a Cu model with a screw dislocation (Fig. S5 in the Supplementary Material).

Solid-solution strengthening is caused by the dislocation-solute atom interaction. We attempted to reveal a relationship between the solid-solution strengthening (i.e.,

mechanical properties) obtained from the MD simulations and the energy profile for the edge dislocation motion under the effect of a solute atom (i.e., energetic properties) obtained by NEB calculations. Fig. 8 shows the relationship between $\Delta\tau_{max}$ and F_{NEB} for Cu-Ni, Cu-Co, and Cu-Mo. The $\Delta\tau_{max}$ values obtained from the models for Cu-Mo with y-axis lengths of $1l$ and $3l$ were used. As shown, $\Delta\tau_{max}$ and F_{NEB} have a linear correlation. The increment in the solid stress component of the depinning stress can be understood from the energy profile of the dislocation motion. The depinning force for the dislocation-Mo interaction in FCC alloys can be predicted using a theoretical model based on the size effect (Fig. 7 (c)). This is useful because the size effect in various alloy systems can be evaluated accurately by first-principles calculations. The SF effect also contributes to solid-solution strengthening when the solute concentration in the SF region is high, as suggested in Fig. 4(b) and Fig. 5(c), (d). In general, first-principles calculations with a high computational cost cannot be used for the NEB analysis of the edge dislocation motion in FCC alloys. Therefore, in this study, we used MEAM potentials to conduct MD simulations at a finite temperature and NEB simulations at 0 K. Hence, this study provides a qualitative understanding of the energy profile for the dislocation motion and relates it to the size effect, SF effect, and interaction energy. The results of our study suggest that the characteristics of the size and SF effects on the energy profile for the edge dislocation

motion, as well as the solid-solution strengthening effect on the edge dislocation motion in various FCC alloys, can be discussed based on a simple theoretical model and quantitative first-principles calculations of the size and SF effects. Therefore, our study can provide an atomistic basis for the design of various FCC alloys for solid-solution strengthening via edge dislocation-solute interactions.

In this study, we discussed the solute effect on the dislocation motion in a dilute solute system. Solute atoms with small size and SF effects can also affect the dislocation motion when the solute concentration is considerably high. In practice, experimental studies have indicated that solute Ni has a small but finite effect on the yield strength of Cu when the Ni concentration is 5 at% [36,37]. In addition, solute atoms may affect the dislocation mobility through two different mechanisms. The first is the solute effect on the dislocation sliding motion on a single slip plane (discussed in this paper). The second is the effect on cross-slip behaviors. For instance, when the solute atom changes the SF energy and dislocation core structure, the frequency of the cross-slip may change. In FCC alloys with a high concentration of solute atoms, this SF effect on the macroscopic mechanical properties in the cross-slip mechanism remains to be elucidated and is a topic for future work.

4. Conclusions

In this study, the energy profile of the edge dislocation motion under the influence of solute atoms with different size and SF effects, as well as the origin of solid-solution strengthening in FCC-Cu alloys, were clarified. We discussed the background physics of the relationship between dislocation-solute atom interactions using qualitative model systems. The obtained results are summarized below, and can serve as a basis for extracting solute atoms that improve the mechanical strength of Cu alloys to facilitate the development of new high-strength Cu alloys.

(1) The maximum shear stress, τ_{max}, required for the dislocation to leave the solute atoms with different size and SF effects was determined by finite temperature MD simulations. Mo with large size and SF effects exhibited a large solid-solution strengthening effect for Cu in the MD shear simulations. A significant interaction between an edge dislocation and one solute Co atom was not observed in Cu-Co. Nevertheless, the simultaneous presence of several solute atoms in the SF region can induce solid-solution strengthening owing to solute-SF interactions.

(2) We evaluated the energy profiles of the edge dislocation motion via the NEB method to investigate the dislocation-solute atom interaction. The NEB results showed that Mo induced considerable changes in the energy profile for the edge dislocation motion owing

to the interaction with partial dislocations. We propose that the change in the energy profile allows us to qualitatively evaluate the force required for depinning (F_{NEB}), which can explain the trend of solid-solution strengthening evaluated by the MD simulations. In other words, the solid-solution-strengthening effect can be connected to the variation in the energy profile for the edge dislocation motion under the effect of solute atoms.

(3) We proposed a validity of the theoretical model that qualitatively predict the depinning force (F_v) based on the size effect and the volumetric strain around the dislocation core. F_v was consistent with F_{NEB} for solute Mo, suggesting that the size misfit was the dominant factor for the dislocation-solute Mo interaction and solid-solution strengthening by Mo.

CRediT authorship contribution statement

Chiharu Kura: Data Curation; Investigation; Writing–original draft preparation. **Masato Wakeda:** Data Curation; Investigation; Writing–original draft preparation.

Kazushi Hayashi: Supervision; Project administration; Writing – review & editing.

Takahito Ohmura: Supervision; Project administration; Writing – review & editing.

Declaration of Competing Interest

The authors declare that they have no known competing financial interests or personal relationships that could have appeared to influence the work reported in this paper.

Data Availability

The data that support the findings of this study are available from the corresponding authors upon reasonable request.

Acknowledgement

Some of the calculations in this study were performed using the Numerical Materials Simulator at the National Institute for Materials Science, Japan.

References

1) F. Kohler, T. Campanella, S. Nakanishi, M. Rappaz, Application of single pan thermal analysis to Cu-Sn peritectic alloys, Acta Mater. 56 (2008) 1519-1528, https://doi.org/10.1016/j.actamat.2007.12.006.

2) G. Li, Z. Hang, S. Yue, Q. Liu, Z. Guo, H. Ding, J. Jie, T. Li, Microstructures and properties of Ni-Si precipitation strengthened phosphor bronze, J. Alloys Compd. 946 (2023) 169388, https://doi.org/10.1016/j.jallcom.2023.169388.

3) H. S. Park, T. Kimura, T. Murakami, Y. Nagano, K. Nakata, M. Ushio, Microstructures and mechanical properties of friction stir welds of 60% Cu–40% Zn copper alloy, Mater. Sci. Eng.: A. 371 (2004) 160-169, https://doi.org/10.1016/j.msea.2003.11.030.

4) A. Heidarzadeh, T. Saeid, A comparative study of microstructure and mechanical properties between friction stir welded single and double phase brass alloys, Mater. Sci. Eng.: A. 649 (2016) 349-358, https://doi.org/10.1016/j.msea.2015.10.012.

5) L. Guo, P. Guo, Z. Zhang, Q. Zhang, M. Zhao, X. Hou, J. Wu, B. Zhang, A review of Cu–Ni–Sn alloys: Processing, microstructure, properties, and developing trends, Materials. 16 (2023) 444, https://doi.org/10.3390/ma16010444.

6) Q. Dong, L. Shen, F. Cao, Y. Jia, K. Liao, M. Wang, Effect of thermomechanical processing on the microstructure and properties of a Cu–Fe–P alloy, J. Mater. Eng. Perform. 4 (2015) 1531-1539, https://doi.org/10.1007/s11665-014-1352-6.

7) M. Murayama, A. Belyakov, T. Hara, Y. Sakai, K. Tsuzaki, M. Okubo, M. Eto, T. Kimura, Development of a high-strength high-conductivity Cu-Ni-P alloy. Part I: characterization of precipitation products, J. Electron. Mater. 35 (2006) 1787-1792, https://doi.org/10.1007/s11664-006-0158-1.

8) D. Hanoz, A.G. Settimi, L. Pezzato, M. Dabala, Effect of precipitation hardening on corrosion resistance of Cu-4.5 wt.%Ti, J. Mater. Eng. Perform. 30 (2021) 1306-1317, https://doi.org/10.1007/s11665-020-05353-0.

9) Q. Gong, J. Liu, F. Wu, H. Chen, W. Xie, H. Wang, B. Yang, Precipitation behavior and strengthening effects of the Cu-0.42Cr-0.16Co alloy during aging treatment, J. Alloys Compd. 936 (2023) 168269, https://doi.org/10.1016/j.jallcom.2022.168269.

10) C. Kura, M. Wakeda, K. Hayashi, T. Ohmura, Energetic and atomic structural analyses of the screw dislocation absorption at tilt grain boundaries in BCC-Fe. Sci. Rep. 12 (2022) 21301, https://doi.org/10.1038/s41598-022-25066-9.

11) M. Wakeda, Y-L. Chang, S. Ii, T. Ohmura, Multiscale analyses of the interaction between dislocation and Σ9 symmetric tilt grain boundaries in Fe–Si bicrystals by

nanoindentation technique, Int. J. Plast. 145 (2021) 103047, https://doi.org/10.1016/j.ijplas.2021.103047.

12) M. Wakeda, T. Ohmura, Atomistic evaluation of the dislocation transmission across tilt and twist low-angle grain boundaries in body-centered cubic iron, Comput. Mater. Sci. 228 (2023) 112335, https://doi.org/10.1016/j.commatsci.2023.112335.

13) Z. Huda, Mechanical Behavior of Materials Fundamentals, Analysis, and Calculations, first ed., Springer, New York, 2021.

14) M. Wakeda, T. Tsuru, M. Kohyama, T. Ozaki, H. Sawada, M. Itakura, S. Ogata, Chemical misfit origin of solute strengthening in iron alloys, Acta. Mater. 131 (2017) 445-456, https://doi.org/10.1016/j.actamat.2017.04.017.

15) T. Tsuru, M. Wakeda, T. Suzudo, M. Itakura, S. Ogata, Anomalous solution softening by unique energy balance mediated by kink mechanism in tungsten-rhenium alloys, J. Appl. Phys. 127 (2020) 025101, https://doi.org/10.1063/1.5131279.

16) T. Kunimine, Y. Tomaru, M. Watanabe, R. Monzen, Tensile deformation behavior of high-strength nanostructured Cu–Si solid-Solution alloys processed by severe plastic deformation, Mater. Trans. 62 (2021) 479-483, https://doi.org/10.2320/matertrans.MT-M2020308.

17) R. L. Fleischer, Substitutional solution hardening, Acta Metall. 11 (1963) 203-209, https://doi.org/10.1016/0001-6160(63)90213-X.

18) M. Lugovy, V. Slyunyayev, M, Brodnikovskyy, Solid solution strengthening in multicomponent fcc and bcc alloys: Analytical approach, Prog. Nat. Sci. 31 (2021) 95-104, https://doi.org/10.1016/j.pnsc.2020.11.006.

19) J. Zhang, Y. Zhang, A. Wang, T. Liang, Z. Mao, B. Su, H. Li, J. Xie, Insight into the influence of alloying elements on the elastic properties and strengthening of copper: A high-throughput first-principles calculations, Metals. 13 (2023) 875, https://doi.org/10.3390/met13050875.

20) Y. Shiihara, Y. Itai, I. Lobzenko, T. Tsuru, Atomic stress state inside fcc and bcc random alloys: A first-principles approach, Front. Mater. 9 (2022) 895626, https://doi.org/10.3389/fmats.2022.895626.

21) K. Tsuzuki, N. Ide, S. Asano, Computer simulation of the elementary process of solid solution hardening in copper alloys, J. Japan Inst. Metals. 66 (2002) 728-734, https://doi.org/10.2320/jinstmet1952.66.7_728.

22) S. I. Rao, C. Woodward, T. A. Parthasarathy, O. Senkov, Atomistic simulations of dislocation behavior in a model FCC multicomponent concentrated solid solution

alloy, Acta. Mater. 134 (2017) 188-194, https://doi.org/10.1016/j.actamat.2017.05.071.

23) Y. Tian, F. Chen, Z. Cui, X. Tian, Effects of atomic size misfit on dislocation mobility in FCC dense solid solution: Atomic simulations and phenomenological modeling, Int. J. Plast. 160 (2023) 103504, https://doi.org/10.1016/j.ijplas.2022.103504.

24) G. Henkelman, H. Jonsson, Improved tangent estimate in the nudged elastic band method for finding minimum energy paths and saddle points, J. Chem. Phys. 113 (2000) 9978-9985, https://doi.org/10.1063/1.1323224.

25) G. Henkelman, B. P. Uberuaga, H. Jonsson, A climbing image nudged elastic band method for finding saddle points and minimum energy paths, J. Chem. Phys. 113 (2000) 9901-9904, https://doi.org/10.1063/1.1329672.

26) H. Jónsson, G. Mills, K. W. Jacobsen, Nudged elastic band method for finding minimum energy paths of transitions, in Classical and Quantum Dynamics in Condensed Phase Simulations, first ed., World Scientific, Singapore, 1998.

27) D. Hull, D. J. Bacon, Introduction to Dislocations, fifth ed., Elsevier, Cambridge, 2011.

28) H. Suzuki, Chemical interaction of solute atoms with dislocations, Science Reposts of the Research Institutes, Tohoku University. Ser. A, Physics Chemistry and Metallurgy. 4 (1952) 322-325, http://hdl.handle.net/10097/26527.

29) H. Suzuki, Segregation of solute atoms to stacking faults, J. Phys. Soc. Jpn. 17 (1962) 322-325, https://doi.org/10.1143/JPSJ.17.322.

30) S. Plimpton, Fast parallel algorithms for short-range molecular dynamics, J. Comp. Phys. 117 (1995) 1-19, https://doi.org/10.1006/jcph.1995.1039.

31) A. Stukowski, Visualization and analysis of atomistic simulation data with OVITO-the Open Visualization Tool, Model. Simul. Mat. Sci. Eng. 18 (2009) 015012, 10.1088/0965-0393/18/1/015012.

32) B-J. Lee, J-H. Shim, A modified embedded atom method interatomic potential for the Cu–Ni system, Calphad. 28 (2004) 125-132, https://doi.org/10.1016/j.calphad.2004.06.001.

33) J. Wang, S-H. Oh, B-J. Lee, Second-nearest-neighbor modified embedded-atom method interatomic potential for Cu-M (M = Co, Mo) binary systems, Comput. Mater. Sci. 178 (2020) 109627, https://doi.org/10.1016/j.commatsci.2020.109627.

34) B. Onat, S. Durukanoğlu, An optimized interatomic potential for Cu–Ni alloys with the embedded-atom method, J. Phys.: Condens. Matter. 26 (2014) 035404, 10.1088/0953-8984/26/3/035404.

35) D. C. Ghosh, R. Biswas, Theoretical calculation of absolute radii of atoms and ions. Part 1. The atomic radii, Int. J. Mol. Sci. 3 (2002) 87-113, https://doi.org/10.3390/i3020087.

36) I. A. Bryukhanov, Dynamics of edge dislocation in Cu–Ni solid solution alloys at atomic scale, Int. J. Plast. 135 (2020) 102834, https://doi.org/10.1016/j.ijplas.2020.102834.

37) Y. Tian, F. Chen, Z. Cui, X. Tian, Effects of atomic size misfit on dislocation mobility in FCC dense solid solution: Atomic simulations and phenomenological modeling, Int. J. Plast. 160 (2023) 103504, https://doi.org/10.1016/j.ijplas.2022.103504.

Figures

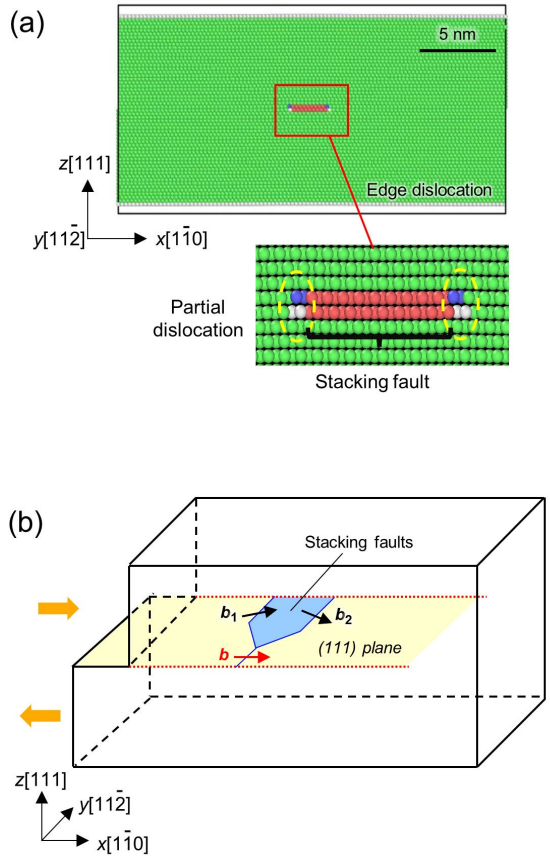

Fig. 1. (a) An atomistic FCC-Cu model containing an edge dislocation. (b) Schematic of the decomposition of an edge dislocation in FCC metals.

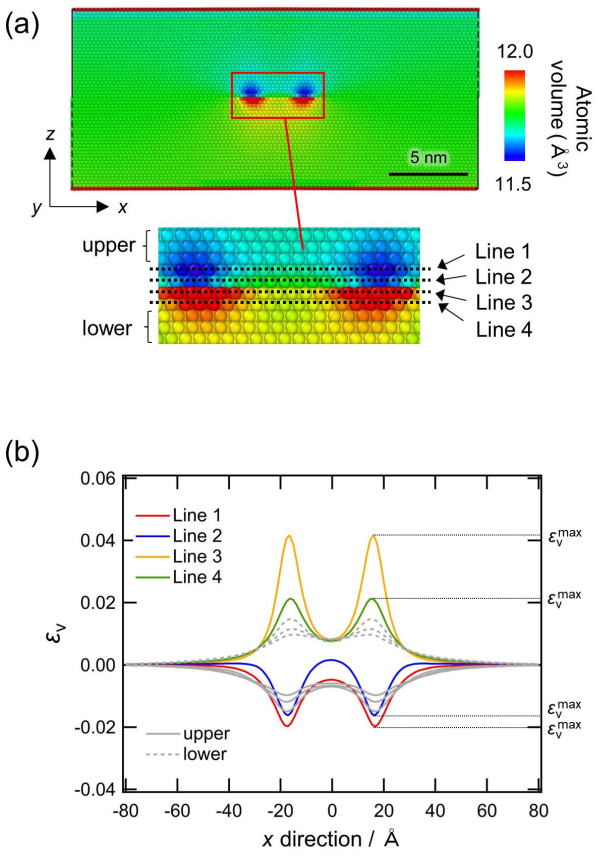

Fig. 2. (a) Visualization of the atomic volume in a Cu model with an edge dislocation. (b) ε_v of Cu atoms in Lines 1-4, upper and lower layers. The center of the model is set to the zero of the *x* coordinate.

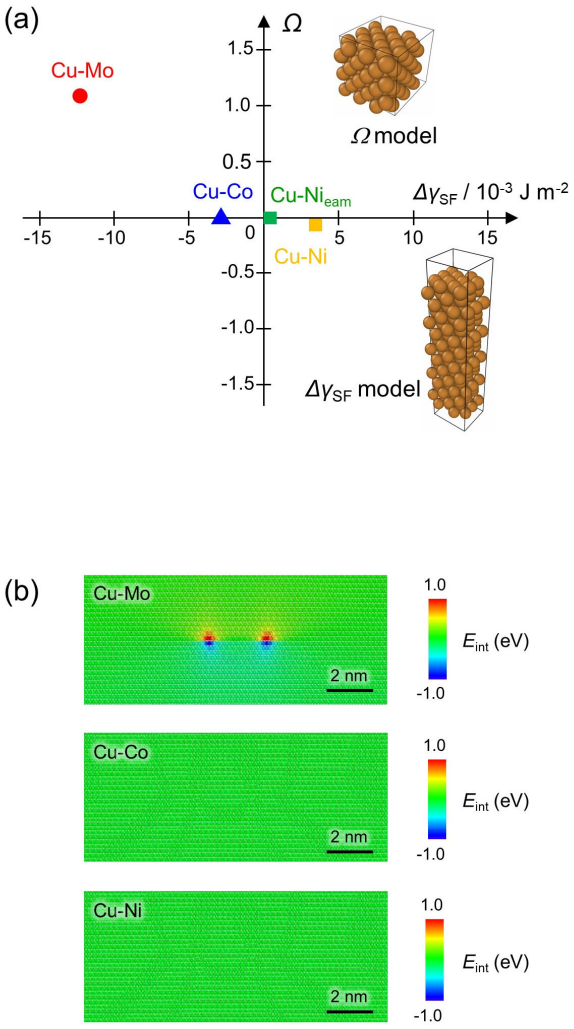

Fig. 3. (a) Size effect (Ω; vertical axis) and solute effect on the SFE ($\Delta\gamma_{SF}$; horizontal axis) diagram of the solute atoms (Ni, Co, and Mo). The inset images show atomic models for Ω and γ_{SF} calculations. (b) Distribution of the interaction energy for solute atoms near the dislocation core.

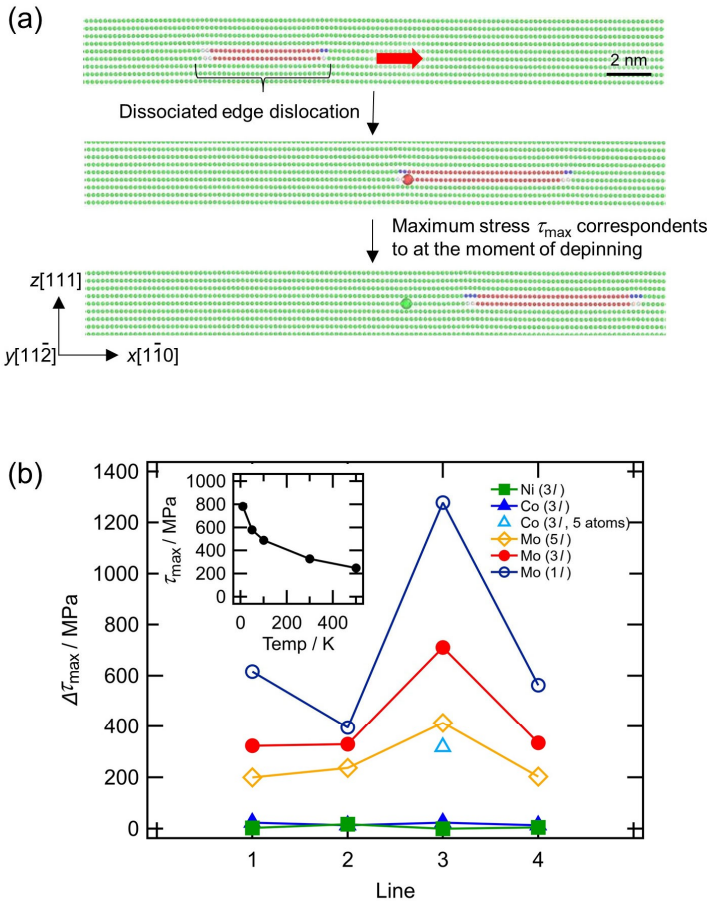

Fig. 4. (a) Dislocation-solute Mo (represented by a large sphere in Line 3) interaction in FCC-Cu. The element colors indicate the crystal structure: FCC (green); hexagonal close-packed (HCP) (red); different crystal structures, such as HCP, icosahedron, and BCC or FCC (white). The red arrow shows the direction of the dislocation motion. (b) $\Delta\tau_{max}$ for the line number where the solute atom is located (defined in Fig. 2(a)). The inset graph shows the temperature dependence of τ_{max} of Cu-Mo for Line 3.

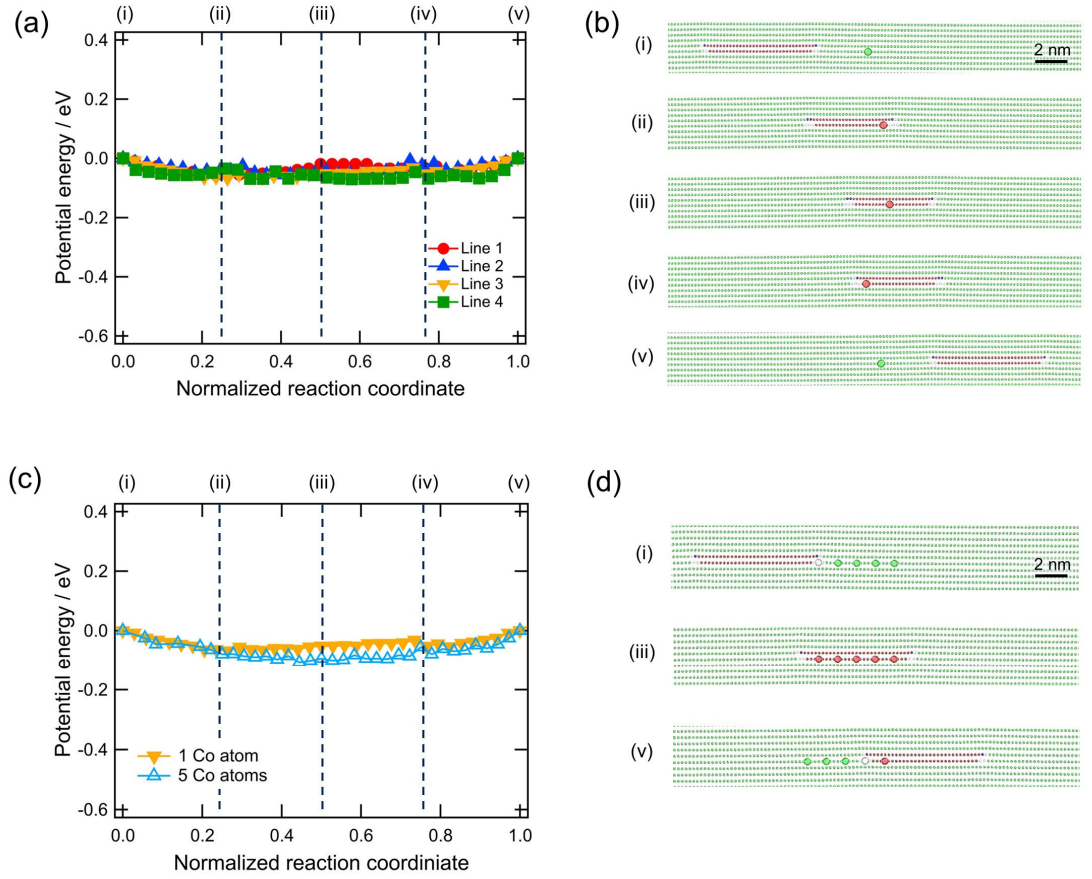

Fig. 5. NEB calculation of the dislocation gliding in Cu-Co. Change in the potential energy profile and visualization of the dislocation gliding for (a), (b) one and (c), (d) five Co atoms. Two NEB simulations were performed, and their results were combined.

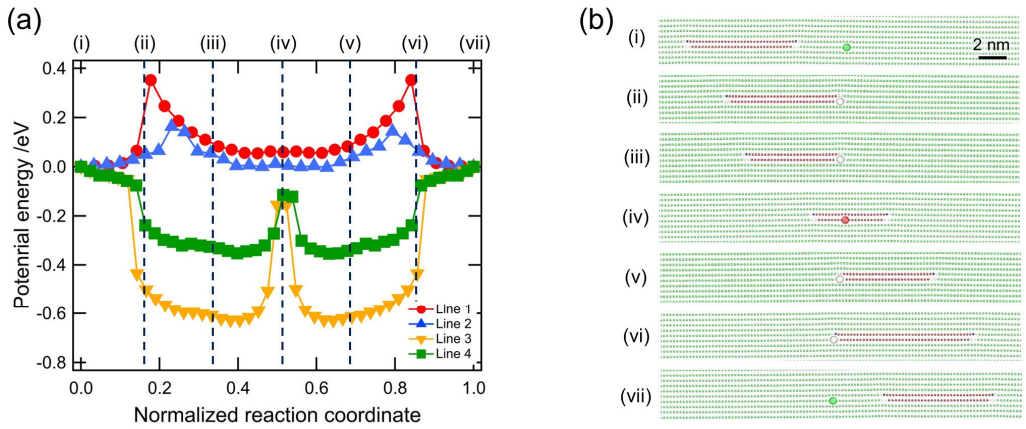

Fig. 6. NEB calculation of the dislocation gliding in Cu-Mo. (a) Change in the potential energy profile and (b) visualization of edge dislocation gliding under the effect of solute Mo on Line 3. Two or three NEB simulations were performed, and their results were combined.

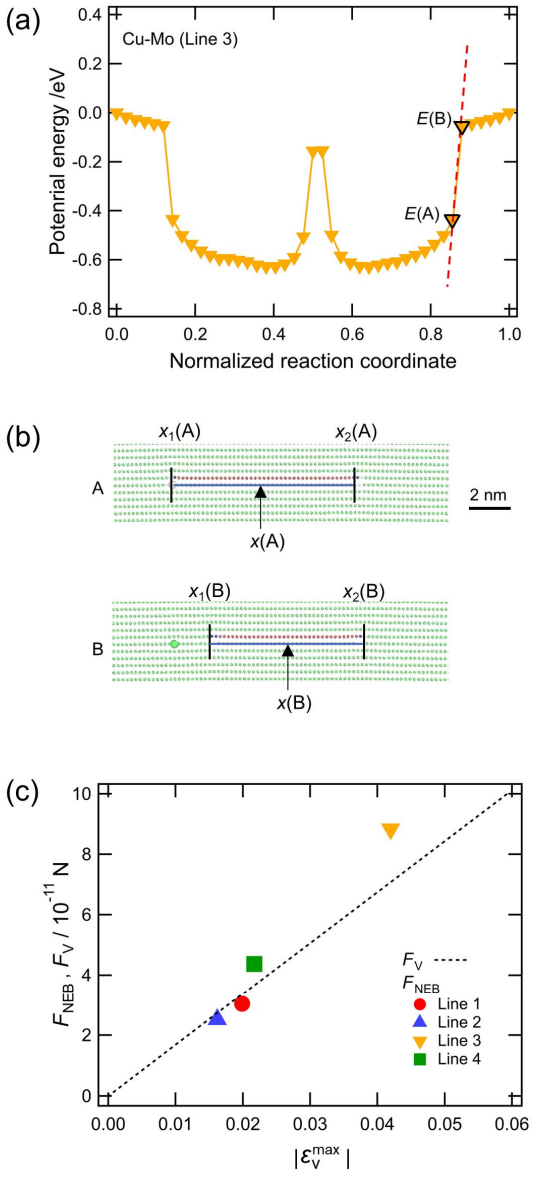

Fig. 7. (a) F_{NEB} evaluation based on the energy profile obtained by NEB simulations. (b) Schematic of the dislocation core position along the *x*-direction. (c) Relationship between F_{NEB}, F_V, and $|\varepsilon_V^{max}|$ for Cu-Mo.

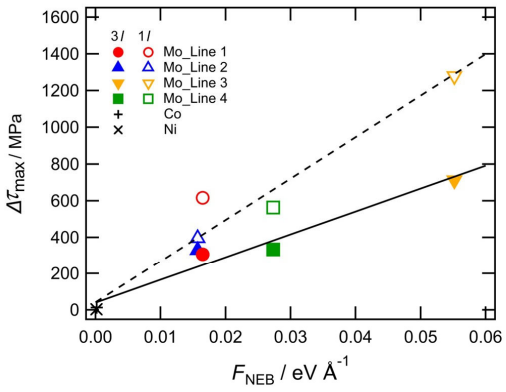

Fig. 8. Relationship between $\Delta\tau_{max}$ and F_{NEB} with y-axis lengths of 3l and 1l. The solid and dashed lines were fitted for each dataset.